HHS Public Access

Author manuscript

*Biol Psychiatry*. Author manuscript; available in PMC 2022 August 15.

Published in final edited form as:

*Biol Psychiatry*. 2021 August 15; 90(4): 263–274. doi:10.1016/j.biopsych.2021.03.023.

# Cyclic-AMP Signaling-Mediated Phosphorylation of Diacylglycerol Lipase α Regulates Interaction with Ankyrin-G and Dendritic Spine Morphology

**Sehyoun Yoon**[1], **Kristoffer Myczek**[1], **Peter Penzes**[1,2,3,4]

[1]Department of Physiology, Northwestern University Feinberg School of Medicine, Chicago, IL 60611, USA

[2]Department of Psychiatry and Behavioral Sciences, Northwestern University Feinberg School of Medicine, Chicago, IL 60611, USA

[3]Department of Pharmacology, Northwestern University Feinberg School of Medicine, Chicago, IL 60611, USA

[4]Northwestern University, Center for Autism and Neurodevelopment, Chicago, IL, 60611, USA

## Abstract

**BACKGROUND:** Diacylglycerol lipase α (DAGLα), a major biosynthetic enzyme for endogenous cannabinoid signaling, has emerged as a risk gene in multiple psychiatric disorders. However, its role in the regulation of dendritic spine plasticity is unclear.

**METHODS:** DAGLα wild-type (WT) or point mutants were overexpressed in primary cortical neurons or human embryonic kidney 293T cells. The effects of mutated variants on interaction, dendritic spine morphology and dynamics were examined by proximity ligation assay or fluorescence recovery after photobleaching. Behavioral tests and immunohistochemistry were performed with ankyrin-G conditional knockout (AnkG cKO) and WT male mice.

**RESULTS:** DAGLα modulates dendritic spine size and density, but the effects of changes in its protein level *vs*. enzymatic activity are different, implicating either 2-arachidonoylglycerol (2-AG)-dependent or independent mechanism. The 2-AG-independent effects are mediated by the interaction of DAGLα with ankyrin-G, a multifunctional scaffold protein implicated in psychiatric disorders. Using superresolution microscopy, we observed that they colocalize in distinct nanodomains, which correlate with spine size. *In situ* Proximity Ligation Assay (PLA) combined with structured illumination microscopy (SIM) reveals that DAGLα phosphorylation upon forskolin treatment enhances the interaction with ankyrin-G in spines, leading to increased

Corresponding author: Peter Penzes, Mailing address: Ward Bldg, Rm 7-174, 303 E Chicago Ave, Chicago, IL 60611, Phone: 312-503-1174, p-penzes@northwestern.edu.

From the Department of Physiology (SY, KM, PP) and Department of Psychiatry and Behavioral Sciences, Department of Pharmacology, Center for Autism and Neurodevelopment (PP) Northwestern University Feinberg School of Medicine, Chicago, Illinois. S.Y. initiated the project and performed all experiments and data analysis unless otherwise stated. K.M. designed the yeast-2-hybrid experiments. P.P. supervised the project and interpreted data.

spine size and decreased DAGLα surface diffusion. AnkG cKO mice show significantly decreased DAGLα-positive neurons in the forebrain. In mice, ankyrin-G is required for forskolin-dependent reversal of depression-related behavior.

**CONCLUSION:** Taken together, *ANK3* and *DAGLA*, both neuropsychiatric disorder genes, interact in a complex to regulate spine morphology. These data reveal novel synaptic signaling mechanisms and potential therapeutic avenues.

### Keywords

ANK3; DAGLα; endocannabinoid; cAMP; proximity ligation assay; structured illumination microscopy

## INTRODUCTION

Abnormalities of spine maturation present in excitatory synapses of cortical pyramidal neurons have emerged as key cellular substrates in the pathogenesis of several psychiatric disorders (1, 2). Altered spine density in cortical pyramidal neurons has been observed in postmortem studies of patients with schizophrenia (SZ), bipolar disorder (BD), and autism spectrum disorder (ASD) (3–5). Changes in spine number and morphology contribute to functional connectivity in synaptic circuits (6) and alterations in neuronal activity change the structure and function of dendritic spines and protein composition of synapses (7).

Diacylglycerol lipase α (DAGLα), which is highly enriched in the nervous system, has emerged as a candidate gene in multiple psychiatric disorders including depressive disorders, anxiety disorders, and ASD (8–11). DAGLα, one of two DAGLs cloned to date (12), is distributed at the spine head and neck in hippocampal pyramidal cells (13) and regulates retrograde synaptic plasticity (14, 15). It is the major biosynthetic enzyme for 2-arachidonoylglycerol (2-AG), an endogenous ligand for cannabinoid receptors. To date, endogenous cannabinoid (eCB) signaling has emerged as an essential pathway for synaptic plasticity in several different cell types and has been implicated in the modulation of mood disorders such as anxiety, depressive behaviors, and fear responses (11, 16–18). However, the role of eCB signaling, DAGLα, and other associated proteins in the regulation of dendritic spine morphology is not fully known.

Genetic studies support synaptic protein genes as key factors in the pathogenesis of neuropsychiatric disorders (19–21) and one of the most strongly associated risk factors for BD in genome-wide association studies (GWAS) are common variants at the *ANK3* gene (encoding ankyrin-G) locus (22, 23). The isoforms of 190/270/480 kDa of ankyrin-G share four conserved domains: an ankyrin repeat domain (ARD), a spectrin-binding domain, a death domain, and a regulatory domain (24). The largest 270/480 kDa isoforms have well-characterized roles at the axon initial segment (AIS) and nodes of Ranvier (25), however, the role of the 190 kDa isoform in the brain is less clear. Ankyrin-G was detected in human and rodent postsynaptic density (PSD) proteins by proteomic analyses (26–28) and we have previously reported that the 190 kDa form of ankyrin-G regulates dendritic spine structure and AMPA receptor (AMPARs)-mediated synaptic transmission (29–31). However,

the mechanisms of ankyrin-G function in spines are still poorly understood because little is known about its protein interactome and the signaling networks that regulate its function.

Here, we show that DAGLα interacts with ankyrin-G to regulate spine head size. Using superresolution microscopy, we find that ankyrin-G and DAGLα are located in distinct nanodomain structures within the spine head and that the number of both ankyrin-G and DAGLα puncta predicts mushroom spine head size. We show that treatment of forskolin, a common reagent used to raise cyclic AMP (cAMP) levels, initiates a signaling cascade leading to DAGLα phosphorylation. This phosphorylation enhances the interaction between DAGLα and ankyrin-G within spine heads, and this is concurrent with an increased size of spine heads and a decreased surface diffusion of DAGLα in the membrane. In addition, the absence of ankyrin-G in the forebrain prevented the ability of forskolin to rescue depression-like behaviors. However, treatment with forskolin rescued decreased anxiety levels in ankyrin-G conditional knockout (AnkG cKO) mice but did not affect abnormal locomotor activity. This novel signaling cascade may have implications for synaptic pathophysiology and behavioral abnormalities in neuropsychiatric disorders.

## METHODS AND MATERIALS

Extended methods are presented in the Supplement.

### Cell Culture and Transfection

High-density cortical neuronal cultures were derived from P0 C57BL/6J (The Jackson Laboratory). They were cultured as previously described (30, 31). All procedures involving animals were approved by the Northwestern University Animal Care and Use Committee.

### Immunocytochemistry and Proximity Ligation Assay (PLA)

Cortical neurons plated on coverslips were transfected at DIV21. All procedures were followed by the manufacturer’s instructions (Sigma; Duolink PLA Fluorescence Protocol).

### Imaging and Image Processing

For the analysis of confocal and structured illumination microscopy (SIM) images from immunostained neurons, the number of puncta within the spine head was quantified manually and recorded. Colocalization highlighter images and Manders’ colocalization coefficients were determined by ImageJ after thresholding.

### Behavioral analysis

To test dose responses by forskolin in WT male mice, vehicle (dimethyl sulfoxide; DMSO) and forskolin (0.1, 0.2, and 0.5 mg/kg) were injected, and open field test and forced swim test were conducted. Vehicle (DMSO) or forskolin (0.2 mg/kg; stock solution, 0.06 mg/ml) was injected into i.p., and each behavioral test was conducted 30 min after injection.

### Statistical Analysis

All statistical tests were performed with GraphPad Prism8. A two-sample comparison was performed using Student's t-test, and multiple comparisons were made using one-way or two-way ANOVA followed by a Bonferroni test. Bar graphs are displayed as mean ± SEM.

## RESULTS

### DAGLα Regulates Spine Morphogenesis

To test whether DAGLα is involved in spine morphogenesis, we utilized RNAi to knockdown DAGLα (shDAGLα) in primary cortical cultured neurons. To determine the impact of DAGLα knockdown on spines, we transfected neurons with shDAGLα and analyzed spine morphology and density. Morphological classification of dendritic spines was performed based on geometrical characteristics of spines in Figure 1A. DAGLα knockdown caused a significant reduction in spine density (Figure 1B and 1D), specifically in mushroom- and thin-type spines. However, the spine head area was not altered by DAGLα knockdown (Figure 1C). This indicated a role for DAGLα in the regulation of spine maintenance. Intriguingly, overexpression of DAGLα showed the same effect as DAGLα knockdown on spine density and no effect on spine head area (Figure 1E–G).

As DAGLα is the key enzyme in the synthesis of 2-AG, we tested whether these effects were due to 2-AG synthesis. To investigate the role of 2-AG synthesized by DAGLα in postsynaptic spine morphogenesis, we treated primary cultured cortical neurons with an inhibitor of DAGLα activity that acutely prevents 2-AG formation, RHC80267 (10 μM, 1 hour). Preventing 2-AG formation induced a significant increase in spine head size, but not density (Figure 1H–J). As a convergent approach, to determine the effect of long-term inhibition of DAGLα, we then utilized a DAGLα activity null mutant, DAGLα$^{D524A}$ (12). Expression of DAGLα$^{D524A}$ for 3 days induced an increase in spine head size and an increase in mushroom type spine density (Figure 1K–M). These data indicate that DAGLα modulates dendritic spine size and density, but the effects of its expression level changes *vs.* enzymatic activity are different. These suggest 2-AG independent, as well as 2-AG dependent roles of DAGLα in spine plasticity.

### The ARD of Ankyrin-G Interacts with C-terminus of DAGLα

The enzymatic activity-independent role of DAGLα in spine plasticity may be mediated by its interacting partner proteins. We have previously performed a yeast-2-hybrid screen with a fragment containing the ankyrin repeats 1–12 (amino acids 35–423) of ankyrin-G (30), and identified the carboxy-terminal (C-terminal) region (amino acids 710–849) of DAGLα as a selected interaction domain (SID) (Figure 2A). Because it has been shown that the short 190 kDa isoform of ankyrin-G modulates excitatory synaptic transmission and the regulation of spine morphology (29), we hypothesized that it might mediate the role of DAGLα in spine maintenance. To determine the interaction sites between ankyrin-G and DAGLα, we conducted immunoprecipitation experiments with three HA-tagged domain fragments of ankyrin-G (amino acids 1–807, 808–1475, 1476–1961) and N-terminal or C-terminal regions of Flag-tagged DAGLα (amino acid 1–528, 529–1044; Flag-DAGLα$^{1-528}$ or Flag-DAGLα$^{529-1044}$) (Figure 2B–C). The C-terminus of DAGLα (Flag-DAGLα$^{529-1044}$) was

found to co-immunoprecipitate with the ARD and spectrin binding domains of ankyrin-G. To test the interaction of ankyrin-G and DAGLα within a cellular context, we employed *in situ* Proximity Ligation Assays (PLA). The PLA signal was significantly decreased when the C-terminal region of DAGLα was deleted (Flag-DAGLα$^{1-528}$) (Figure 2E). These data suggest that the C-terminal region of DAGLα has an important role in the interaction of ankyrin-G.

## Ankyrin-G and DAGLα Localization in Spine Heads Correlates to Spine Morphology

Because both ankyrin-G and DAGLα have been detected in the PSD by proteomics (28), we hypothesized that their interaction might have a role in regulating spine morphology. Because of the limited resolution of confocal microscopy, we utilized SIM to analyze the precise postsynaptic localization of ankyrin-G and DAGLα (Figure 2F). Interestingly, ankyrin-G nanodomains overlapping with DAGLα localized to both the dendritic shaft and spine head (Figure 2G). Puncta of ankyrin-G or DAGLα were observed in 39.3% and 55.3% of spines, respectively. Both ankyrin-G and DAGLα were observed in 28.3% of spines (Figure 2H–I). Also, the presence of ankyrin-G or DAGLα in spine heads was significantly correlated to larger spine head size (Figure 2J–L), and the presence of both ankyrin-G and DAGLα in spines was correlated to further increased head size (Figure 2I). Taken together, these data show that the size of DAGLα clusters in the spine head is positively correlated to the size of ankyrin-G puncta, and these are both correlated to spine head size.

## Forskolin Enhances the Interaction of DAGLα and Ankyrin-G

To characterize the ankyrin-G/DAGLα interaction *in vivo*, we next examined them in the context of a native mouse brain tissue. To identify ankyrin-G-DAGLα co-expression patterns in the forebrain, we examined their expression by immunofluorescent staining of the mouse primary somatosensory cortex (Bregma, 0.50 mm) and CA3 of the hippocampus (Figure 3A). The overlap between ankyrin-G and DAGLα was strongest in dendritic areas rather than the AIS (Figure 3B). Previous studies showed that phosphorylation motifs of target interactors are important for the modulation of ankyrin-G interaction (30–34). DAGLα contains multiple consensus phosphorylation motifs, including those targeted by the cyclic AMP-dependent protein kinase (PKA) and calmodulin-dependent protein kinase II (Camk2) (35, 36). In addition, mass spectrometry studies support direct evidence for 14 serine/threonine phosphorylation sites in the SID of C-terminal region of DAGLα (amino acids 710–849) (37). Therefore, we hypothesized that post-translational modification (PTM) of the C-terminal region of DAGLα might alter its interaction affinity with ankyrin-G and be responsible for the observed alterations in the spine area and density. After treating 12-week old male mice with forskolin (30 μM) for 30 minutes, we performed co-immunoprecipitation experiments from mouse cortical homogenates. The local expression levels of both ankyrin-G and DAGLα in the membrane and peripheral membrane were not altered by treatment with forskolin (Supplemental Figure 3C–D). Interestingly, forskolin treatment resulted in a significant increase in ankyrin-G/DAGLα interaction, as assessed by reciprocal immunoprecipitations (Figure 3C). To confirm that forskolin-induced enhancement of the ankyrin-G/DAGLα interaction relied on the previously isolated interaction domains (Figure 2), we conducted immunoprecipitation experiments *in vitro*. As observed within the mouse cortex, forskolin treatment in HEK293T cells enhanced the interaction of the

C-terminal region of DAGLα with ankyrin-G in the ARD (Figure 3D). Consistent with this, upregulation of ankyrin-G/DAGLα complex formation was confirmed using PLA in HEK293T cells following forskolin treatment (Supplemental Figure 3E–F). To assess the local interaction of ankyrin-G/DAGLα within neurons, we analyzed PLA signals from endogenous ankyrin-G and DAGLα interaction in the dendrite. The PLA signal was significantly increased both in spine necks and heads following forskolin stimulation (Figure 3E–F). As with the overexpression in HEK293T cells, primary cultured cortical neurons were co-transfected with HA-AnkG and Flag-DAGLα (Supplemental Figure 3H), and the effect of forskolin on CREB phosphorylation was confirmed (Supplemental Figure 3G). The number of PLA puncta increased in both the soma and dendrites significantly (Figure 3G). These results strongly implicate the regulation of the ankyrin-G and DAGLα interaction as a downstream effect following cAMP elevation.

## Forskolin Induces Phosphorylation of DAGLα via PKA

cAMP elevation within neurons activates a host of cellular pathways that may result in PTM of DAGLα. We next aimed to isolate the exact sites involved in cAMP elevation-mediated phosphorylation of DAGLα, and the responsible kinase. To identify DAGLα phosphorylation sites, we incubated Flag-DAGLα$^{529-1044}$ overexpressing HEK293T cells with forskolin. Following immunoprecipitation of Flag-DAGLα$^{529-1044}$, LC-MS/MS analysis of proteolytic digests detected five phosphorylated serine or threonine residues (Ser738, Ser808, Ser954, Ser956, and Thr1023) that exhibited potential cAMP consensus phosphorylation motifs (Table 1). To characterize the potential role of PKA in mediating DAGLα phosphorylation within the C-terminal region, HEK293T cells expressing Flag-DAGLα$^{529-1044}$ were pretreated with an inhibitor of PKA. Rp-8-Br-cAMP is a well-known antagonist for PKAs, more effectively antagonizing PKA type I, by which is resistant against cyclic nucleotide-dependent phosphodiesterases. IP-LC-MS/MS revealed that treatment of Rp-8Br-cAMP followed by cAMP elevation blocked all serine sites but only one threonine site. These results suggest that PKA may phosphorylate DAGLα within the C-terminal region, providing a potential mechanism underlying the cAMP-mediated increase in ankyrin-G/DAGLα interaction.

## Forskolin-mediated Phosphorylation of DAGLα via Serine 738 Enhances the Interaction with Ankyrin-G and Regulates Spine Morphology

To assess the functional outcome of this phosphorylation on ankyrin-G/DAGLα complex formation, phospho-mimetic mutagenesis of these C-terminal sites was carried out. Four serine sites were modified to glutamic acid as phospho-mimetic mutations (S738E, S808E, S954E, S956E) and transfected into HEK293T cells, alongside ankyrin-G. Interestingly, whereas the phospho-mimetic S738E Flag-DAGLα construct showed increased levels of co-IP, suggesting a robust enhancement in the interaction between HA-AnkG$^{1-807}$ and Flag-DAGLα$^{529-1044}$, S808E, S954E, and S956E showed no noticeable ability to enhance the interaction (Supplemental Figure 4A and 4C). To define the requirement of phosphorylation in mediating this increase in interaction, phospho-null mutation of each serine site to alanine (S738A, S808A, S954A, S956A) was performed. Although HA-AnkG$^{1-807}$ was observed to co-IP strongly with Flag-DAGLα$^{529-1044}$ following forskolin stimulation, this interaction was drastically reduced for S738A, and S808A, S954A, S956A showed no change in co-IP

efficiency (Supplemental Figure 4B and 4D). These results show that S738 phosphorylation is sufficient and necessary for forskolin-mediated potentiation of the ankyrin-G/DAGLα interaction. To test the effects of this PTM on the ankyrin-G/DAGLα interaction within a cellular context, *in situ* PLA was employed. Primary cultured neurons were transfected with HA-AnkG and Flag-DAGLα and observed following forskolin or control stimulation. Stronger PLA signals were observed in S738E than wild-type (WT) in the dendritic shafts (Figure 4A–B). Additionally, the PLA signal was significantly increased in both the dendritic shafts and spines after forskolin treatment. However, forskolin-induced PLA signal was abrogated when the phospho-null S738A was employed (Figure 4C–D). To understand the link between spine head size and density, we analyzed the nanodomains of Flag-DAGLα with the measurement of spine head size based on SIM images from Figure 4E and 4H. The expression of phospho-mimetic DAGLα significantly increases the size of spine heads and the presence of DAGLα in spines (Figure 4F–G). Forskolin treatment increased the ratio of DAGLα expressing spines co-incident with an increase in spine density, and it prompted an increase in spine head size (Figure 4H–J). Notably, this upregulation was absent in phospho-null DAGLα transfected cells (Figure 4I–J). Taken together, forskolin-mediated phosphorylation of the serine 738 of DAGLα enhances the interaction between ankyrin-G and DAGLα, an effect that may underlie the functional outcomes on dendritic spine area and density.

## Ankyrin-G Regulates pSer738-mediated Surface Diffusion of DAGLα

A previous report showed that the interaction between ankyrin-G and Nav1.2 sodium channels is modulated by protein kinase CK2-mediated phosphorylation of the ankyrin-binding motif of Nav1.2 (38). Furthermore, a phospho-null mutation in Nav1.2 decreases binding affinity for ankyrin-G and increases diffusion dynamics in the membrane. In addition, phosphorylation of the FIGQY motif tyrosine, which is a highly conserved sequence in the cytoplasmic domains of all members of the L1 family of neural cell adhesion molecules, abolishes ankyrin-G binding and increases lateral mobility (32). Taken together, we hypothesize that forskolin acts to regulate DAGLα surface dynamics by enhancing the interaction with ankyrin-G. To test the effect of ankyrin-G on the surface diffusion of DAGLα, we generated a superecliptic pHluorin (SEP)-DAGLα by inserting SEP into the first extracellular domain (Supplemental Figure 5A). We determined fluorescence recovery after photobleaching (FRAP) of SEP-DAGLα to measure membrane-bound DAGLα mobility in dendritic shafts (Figure 5A). Forskolin treatment reduced the amount of SEP-DAGLα fluorescence recovery in spines compared with control neurons, and the calculation of the total mobile fraction of SEP-DAGLα in each condition revealed a 25% decrease in SEP-DAGLα mobility 10 min after photobleaching (Figure 5B–C). Interestingly, the phospho-mimetic construct (S738E) decreased fluorescence recovery levels (16%), an effect absent in the phospho-null mutant (S738A) (Figure 5D–E). To assess whether these alterations were specific to ankyrin-G, we examined the effect of forskolin on the surface diffusion of DAGLα with the knockdown of ankyrin-G. The knockdown of ankyrin-G attenuated the decreased level of surface diffusion after forskolin treatment (Figure 5F–H). In addition, the phospho-null mutant (S738A) showed similar attenuation in decreased fluorescence recovery after the treatment with forskolin (Figure 5I–K). These

results suggest that the enhanced interaction between ankyrin-G and DAGLα induced by phosphorylation of Ser738 reduces surface diffusion of DAGLα.

### Absence of Ankyrin-G Alters Behavioral Responses Induced by Forskolin

Previous studies have reported that AnkG cKO mice present with hyperactivity as well as decreased anxiety-like and depression-like behaviors (39). To investigate whether the molecular modifications and cellular alterations described above were also associated with anatomical and behavioral phenotypes relevant to neuropsychiatric disorders, we analyzed AnkG cKO mice with specific disruption of *ANK3* in pyramidal neurons of the adult forebrain. Immunohistological analysis of AnkG cKO mice showed significant decreases in the total number of DAGLα-positive cells in layer V of the cortex and CA3 of the hippocampus as compared to wild-type (Figure 6A–B). Also, dendritic expression of DAGLα in layer V was significantly reduced in AnkG cKO mice (Supplemental Figure 7A–B). Western blotting, however, showed unaltered DAGLα protein level in P2 membrane fractions (Supplemental Figure 7C–D).

Previous studies showed that the level of cAMP in the brain was altered in major depressive disorder (40). In addition, phosphodiesterase-4 (PDE4), an enzyme for the hydrolysis of cAMP, has been investigated as a target for the treatment of depression (41). As such, we investigated whether and how previously-reported behavioral phenotypes in AnkG cKO mice were affected by forskolin treatment. As in wild-type mice, forskolin treatment (0.2 mg/kg) did not affect locomotor activity in AnkG cKO mice, suggesting that the effects in other behavioral tests were not due to effects on overall mobility (Figure 6C). We then assessed phenotypes related to depression and anxiety in the forced swim, light/dark box, and zero maze tests (39). While forskolin treatment reduced immobile time in wild-type controls, it did not affect AnkG cKO mice (Figure 6D). This indicates that ankyrin-G is required for the effect of forskolin on depression-related behavioral phenotypes. On the contrary, however, the decreased anxiety-like behavior observed in the zero maze and light/dark box tests was reversed by forskolin in AnkG cKO mice, while the behavior in WT mice was not affected by forskolin treatment (Figure 6E–F). These data suggest that forskolin treatment can rescue in AnkG cKO mice behavioral phenotypes relevant for anxiety, but not those relevant for depression, and that these effects of forskolin may be mediated by the ankyrin-G/DAGLα interaction in specific brain circuits.

## DISCUSSION

DAGLα has emerged as a candidate gene in multiple psychiatric disorders including depressive disorders, anxiety disorders, and ASD (8–11). These disorders share common synaptic pathologies, such as alterations in synaptic number and size; however, little is known about the underlying molecular mechanisms. Immunoprecipitation of anti-DAGLα-associated protein complexes from mouse striatum revealed that 23 out of 25 interacting proteins were PSD-related, including Shank3, Anks1b, Homer1, and Camk2α (9). Here, we show that ankyrin-G is a novel DAGLα interacting partner, regulating surface diffusion during spine enlargement within excitatory neurons. SIM identified the localization of ankyrin-G and DAGLα nanodomains in spine heads and revealed correlations between the

presence of nanodomains and spine head size. In addition, cAMP signaling induces the phosphorylation of the C-terminal region of DAGLα, resulting in enhanced interaction with ankyrin-G.

SIM has been instrumental in showing that ankyrin-G is localized to perisynaptic regions (29). In particular, the combination of SIM with PLA (PLA-SIM) provides an unprecedented ability to examine protein-protein interactions at the nanoscale level. Here we show that the interaction of ankyrin-G with DAGLα occurs primarily in a region of the spine head facing the interior of the spine. In addition, a newly generated SEP-DAGLα construct allowed the analysis of surface diffusion of membrane-bound DAGLα. This tool allowed us to reveal that surface dynamics play an integral role in DAGLa mediated regulation of dendritic spine morphology, opening new avenues in the study of DAGLa in neuronal biology.

DAGLα (containing 1044 amino acids) is longer than its analog, DAGLβ (669 amino acids). Variants in the substantially longer C-terminal tail in *DAGL*α are highly associated with multiple neurodevelopmental disorders, such as epilepsy, developmental delay, intellectual disability, and ASD (8). Here, LC-MS/MS revealed a novel mechanism involving the cAMP signaling pathway. Inhibition of PKA blocked the phosphorylation of serine 738, 808, 954, and 956 induced by forskolin (Table 1); however, only phosphorylated serine 738 was involved in modulation of the ankyrin-G interaction (Figure 4 and Supplemental Figure 4). This is a novel finding for the role of ankyrin-G in eCB pathways and implicates that ankyrin-G and DAGLα, both psychiatric risk factors, share a common cAMP pathway. Regulation of this pathway may have therapeutic benefit in disorder states linked to altered ankyrin-G and DAGLα expression.

We found that the C-terminal region of DAGLα-mediated a putative non-retrograde pathway that regulates dendritic spine development through interaction with ankyrin-G. Moreover, cAMP-mediated phosphorylation of serine 738 of DAGLα enhanced the interaction with ankyrin-G and regulated spine morphology. These results suggest that cAMP-mediated acute spine enlargement is modulated through a postsynaptic mechanism independent of retrograde eCB signaling. However, we surprisingly found that overexpression and knockdown of DAGLα caused the same effect on spine density and no effect on spine head area. Moreover, we observed that both short- and long-term inhibition of DAGLα (i.e., inhibition of 2-AG formation) affected spine enlargement. These data suggest that several different mechanisms may underlie the role of DAGLα in spines. One may be an enzymatic-independent mechanism, not involving retrograde eCB signaling, but instead dependent on the C-terminal region of DAGLα interacting with ankyrin-G. The other may be an enzymatic activity-dependent mechanism, in which DAGLα may control the homeostatic regulation of spine size and density in a bell-shaped effect manner. Further investigations using agonists or antagonists of the eCB signaling pathway are necessary to identify the precise mechanism.

Here we identify a novel mechanism for limiting DAGLα surface diffusion: forskolin-mediated enhancement of the ankyrin-G/DAGLα interaction increased DAGLα immobilization at the membrane of dendrites. Because DAGLα is localized on postsynaptic spine heads closely apposed to presynaptic CB1R-bearing axon terminals (13, 42) and

2-AG severely limits its diffusion in the extracellular space (43), DAGLα surface diffusion could affect eCB-mediated pre- and postsynaptic plasticity. Furthermore, our previous study showed that ankyrin-G regulates AMPARs surface dynamics (29), and another group reported that DAGLα mediates group I metabotropic glutamate receptors (mGluRs)-induced 2-AG mobilization through the association of both with Homer1b (44). We speculate that the association or dissociation of these large protein complexes might play a role in eCB-mediated pre- and postsynaptic plasticity.

We found that in mice, conditional deletion of ankyrin-G causes a reduction in DAGLα positive neurons in the layer V of cortex and the CA3 of hippocampus, but does not reduce the overall membrane association in P2 fractions. These suggest that DAGLα may be uncoupled from cytoskeletal effectors and redistributed along the membrane. Importantly, ankyrin-G was required for the rescuing effect of forskolin on depression-related behavior. On the contrary, abnormal anxiety-like behaviors in AnkG cKO mice could be reversed by forskolin, suggesting a role for cAMP/PKA-mediated pathways in reversal. Notably, DAGLα knockout mice showed alterations in anxiety and depressive behaviors (10, 17). Nonetheless, ankryrin-G as a scaffold protein interacts with PSD proteins, and forskolin-mediated responses in AnkG cKO mice may be altered by other pathways. Further investigations using a knock-in mouse model expressing a phospho-mimetic or -null mutation of DAGLα are necessary to understand the fine mechanism. A limitation of our study was that it only included male mice. As some phenotypes may be different by sex, future studies comparing female and male mice would be important.

Our findings demonstrate that interaction between the C-terminal region of DAGLα and ankyrin-G regulates spine morphogenesis. Studying these pathways may help elucidate the molecular mechanisms and structural deficits that correlate to various psychiatric disorders and highlight novel directions in understanding the physiological and translational pathways involved in the etiology of psychiatric disease.

## Supplementary Material

Refer to Web version on PubMed Central for supplementary material.

## ACKNOWLEDGMENTS AND DISCLOSURES

This work was supported by R01MH107182 to P.P. We thank to the Center for Advanced Microscopy and the Behavioral Phenotyping Core facilities at NU for the use of the N-SIM and behavioral tests, respectively.

The authors report no biomedical financial interests or potential conflicts of interest.

## REFERENCES

1. Penzes P, Cahill ME, Jones KA, VanLeeuwen JE, Woolfrey KM (2011): Dendritic spine pathology in neuropsychiatric disorders. Nature Neuroscience. 14:285–293. [PubMed: 21346746]
2. Forrest MP, Parnell E, Penzes P (2018): Dendritic structural plasticity and neuropsychiatric disease. Nat Rev Neurosci. 19:215–234. [PubMed: 29545546]
3. Glantz LA, Lewis DA (2000): Decreased dendritic spine density on prefrontal cortical pyramidal neurons in schizophrenia. Arch Gen Psychiat. 57:65–73. [PubMed: 10632234]

4. Hutsler JJ, Zhang H (2010): Increased dendritic spine densities on cortical projection neurons in autism spectrum disorders. Brain Res. 1309:83–94. [PubMed: 19896929]
5. Konopaske GT, Lange N, Coyle JT, Benes FM (2014): Prefrontal Cortical Dendritic Spine Pathology in Schizophrenia and Bipolar Disorder. Jama Psychiat. 71:1323–1331.
6. Bosch M, Hayashi Y (2012): Structural plasticity of dendritic spines. Curr Opin Neurobiol. 22:383–388. [PubMed: 21963169]
7. Makino H, Malinow R (2009): AMPA Receptor Incorporation into Synapses during LTP: The Role of Lateral Movement and Exocytosis. Neuron. 64:381–390. [PubMed: 19914186]
8. Smith DR, Stanley CM, Foss T, Boles RG, McKernan K (2017): Rare genetic variants in the endocannabinoid system genes CNR1 and DAGLA are associated with neurological phenotypes in humans. Plos One. 12.
9. Shonesy BC, Wang X, Rose KL, Ramikie TS, Cavener VS, Rentz T, et al. (2013): CaMKII regulates diacylglycerol lipase-alpha and striatal endocannabinoid signaling. Nat Neurosci. 16:456–463. [PubMed: 23502535]
10. Powell DR, Gay JP, Wilganowski N, Doree D, Savelieva KV, Lanthorn TH, et al. (2015): Diacylglycerol lipase a knockout mice demonstrate metabolic and behavioral phenotypes similar to those of cannabinoid receptor 1 knockout mice. Front Endocrinol. 6.
11. Jenniches I, Ternes S, Albayram O, Otte DM, Bach K, Bindila L, et al. (2016): Anxiety, Stress, and Fear Response in Mice With Reduced Endocannabinoid Levels. Biol Psychiatry. 79:858–868. [PubMed: 25981172]
12. Bisogno T, Howell F, Williams G, Minassi A, Cascio MG, Ligresti A, et al. (2003): Cloning of the first sn1-DAG lipases points to the spatial and temporal regulation of endocannabinoid signaling in the brain. J Cell Biol. 163:463–468. [PubMed: 14610053]
13. Yoshida T, Fukaya M, Uchigashima M, Miura E, Kamiya H, Kano M, et al. (2006): Localization of diacylglycerol lipase-alpha around postsynaptic spine suggests close proximity between production site of an endocannabinoid, 2-arachidonoyl-glycerol, and presynaptic cannabinoid CB1 receptor. J Neurosci. 26:4740–4751. [PubMed: 16672646]
14. Gao Y, Vasilyev DV, Goncalves MB, Howell FV, Hobbs C, Reisenberg M, et al. (2010): Loss of Retrograde Endocannabinoid Signaling and Reduced Adult Neurogenesis in Diacylglycerol Lipase Knock-out Mice. J Neurosci. 30:2017–2024. [PubMed: 20147530]
15. Tanimura A, Yamazaki M, Hashimotodani Y, Uchigashima M, Kawata S, Abe M, et al. (2010): The Endocannabinoid 2-Arachidonoylglycerol Produced by Diacylglycerol Lipase alpha Mediates Retrograde Suppression of Synaptic Transmission. Neuron. 65:320–327. [PubMed: 20159446]
16. Valverde O, Torrens M (2012): CB1 receptor-deficient mice as a model for depression. Neuroscience. 204:193–206. [PubMed: 21964469]
17. Shonesy BC, Bluett RJ, Ramikie TS, Baldi R, Hermanson DJ, Kingsley PJ, et al. (2014): Genetic Disruption of 2-Arachidonoylglycerol Synthesis Reveals a Key Role for Endocannabinoid Signaling in Anxiety Modulation. Cell Rep. 9:1644–1653. [PubMed: 25466252]
18. Khan MA, Akella S (2009): Cannabis-induced bipolar disorder with psychotic features: a case report. Psychiatry (Edgmont). 6:44–48. [PubMed: 20104292]
19. Gilman SR, Iossifov I, Levy D, Ronemus M, Wigler M, Vitkup D (2011): Rare De Novo Variants Associated with Autism Implicate a Large Functional Network of Genes Involved in Formation and Function of Synapses. Neuron. 70:898–907. [PubMed: 21658583]
20. Nurnberger JI, Koller DL, Jung J, Edenberg HJ, Foroud T, Guella I, et al. (2014): Identification of Pathways for Bipolar Disorder A Meta-analysis. Jama Psychiat. 71:657–664.
21. Purcell SM, Moran JL, Fromer M, Ruderfer D, Solovieff N, Roussos P, et al. (2014): A polygenic burden of rare disruptive mutations in schizophrenia. Nature. 506:185–+. [PubMed: 24463508]
22. Ferreira MAR, O'Donovan MC, Meng YA, Jones IR, Ruderfer DM, Jones L, et al. (2008): Collaborative genome-wide association analysis supports a role for ANK3 and CACNA1C in bipolar disorder. Nat Genet. 40:1056–1058. [PubMed: 18711365]
23. Schulze TG, Detera-Wadleigh SD, Akula N, Gupta A, Kassem L, Steele J, et al. (2009): Two variants in Ankyrin 3 (ANK3) are independent genetic risk factors for bipolar disorder. Mol Psychiatr. 14:487–491.

24. Mohler PJ, Bennett V (2005): Defects in ankyrin-based cellular pathways in metazoan physiology. Front Biosci. 10:2832–2840. [PubMed: 15970537]
25. Bennett V, Healy J (2008): Organizing the diseases fluid membrane bilayer: diseases linked to spectrin and ankyrin. Trends Mol Med. 14:28–36. [PubMed: 18083066]
26. Jordan BA, Fernholz BD, Boussac M, Xu CF, Grigorean G, Ziff EB, et al. (2004): Identification and verification of novel rodent postsynaptic density proteins. Mol Cell Proteomics. 3:857–871. [PubMed: 15169875]
27. Collins MO, Husi H, Yu L, Brandon JM, Anderson CNG, Blackstock WP, et al. (2006): Molecular characterization and comparison of the components and multiprotein complexes in the postsynaptic proteome. J Neurochem. 97:16–23. [PubMed: 16635246]
28. Bayes A, Collins MO, Croning MDR, van de Lagemaat LN, Choudhary JS, Grant SGN (2012): Comparative Study of Human and Mouse Postsynaptic Proteomes Finds High Compositional Conservation and Abundance Differences for Key Synaptic Proteins. Plos One. 7.
29. Smith KR, Kopeikina KJ, Fawcett-Patel JM, Leaderbrand K, Gao RQ, Schurmann B, et al. (2014): Psychiatric Risk Factor ANK3/Ankyrin-G Nanodomains Regulate the Structure and Function of Glutamatergic Synapses. Neuron. 84:399–415. [PubMed: 25374361]
30. Yoon S, Parnell E, Kasherman M, Forrest MP, Myczek K, Premarathne S, et al. (2019): Usp9X Controls Ankyrin-Repeat Domain Protein Homeostasis during Dendritic Spine Development. Neuron.
31. Yoon S, Parnell E, Penzes P (2020): TGF-beta-Induced Phosphorylation of Usp9X Stabilizes Ankyrin-G and Regulates Dendritic Spine Development and Maintenance. Cell Rep. 31:107685. [PubMed: 32460012]
32. Garver TD, Ren Q, Tuvia S, Bennett V (1997): Tyrosine phosphorylation at a site highly conserved in the L1 family of cell adhesion molecules abolishes ankyrin binding and increases lateral mobility of neurofascin. J Cell Biol. 137:703–714. [PubMed: 9151675]
33. Zhang X, Davis JQ, Carpenter S, Bennett V (1998): Structural requirements for association of neurofascin with ankyrin. J Biol Chem. 273:30785–30794. [PubMed: 9804856]
34. Jenkins SM, Kizhatil K, Kramarcy NR, Sen A, Sealock R, Bennett V (2001): FIGQY phosphorylation defines discrete populations of L1 cell adhesion molecules at sites of cell-cell contact and in migrating neurons. J Cell Sci. 114:3823–3835. [PubMed: 11719549]
35. Reisenberg M, Singh PK, Williams G, Doherty P (2012): The diacylglycerol lipases: structure, regulation and roles in and beyond endocannabinoid signalling. Philos T R Soc B. 367:3264–3275.
36. Shonesy BC, Stephenson JR, Marks CR, Colbran RJ (2020): Cyclic AMP-dependent protein kinase and D1 dopamine receptors regulate diacylglycerol lipase-alpha and synaptic 2-arachidonoyl glycerol signaling. J Neurochem.
37. Hornbeck PV, Zhang B, Murray B, Kornhauser JM, Latham V, Skrzypek E (2015): PhosphoSitePlus, 2014: mutations, PTMs and recalibrations. Nucleic Acids Res. 43:D512–520. [PubMed: 25514926]
38. Brachet A, Leterrier C, Irondelle M, Fache MP, Racine V, Sibarita JB, et al. (2010): Ankyrin G restricts ion channel diffusion at the axonal initial segment before the establishment of the diffusion barrier. J Cell Biol. 191:383–395. [PubMed: 20956383]
39. Zhu S, Cordner ZA, Xiong J, Chiu CT, Artola A, Zuo Y, et al. (2017): Genetic disruption of ankyrin-G in adult mouse forebrain causes cortical synapse alteration and behavior reminiscent of bipolar disorder. Proc Natl Acad Sci U S A. 114:10479–10484. [PubMed: 28894008]
40. Fujita M, Richards EM, Niciu MJ, Ionescu DF, Zoghbi SS, Hong J, et al. (2017): cAMP signaling in brain is decreased in unmedicated depressed patients and increased by treatment with a selective serotonin reuptake inhibitor. Mol Psychiatr. 22:754–759.
41. Zhang HT, Wang H, Zhang FF, Li B, Zhou YM, Yu HY, et al. (2019): Inhibition of phosphodiesterase-4D reverses memory deficits and depression-like effects via cAMP signaling in mouse models of Alzheimer's disease. Faseb J. 33.
42. Katona I, Urban GM, Wallace M, Ledent C, Jung KM, Piomelli D, et al. (2006): Molecular composition of the endocannabinoid system at glutamatergic synapses. J Neurosci. 26:5628–5637. [PubMed: 16723519]

43. Zou SL, Kumar U (2018): Cannabinoid Receptors and the Endocannabinoid System: Signaling and Function in the Central Nervous System. Int J Mol Sci. 19.

44. Jung KM, Astarita G, Zhu C, Wallace M, Mackie K, Piomelli D (2007): A key role for diacylglycerol lipase-alpha in metabotropic glutamate receptor-dependent endocannabinoid mobilization. Mol Pharmacol. 72:612–621. [PubMed: 17584991]

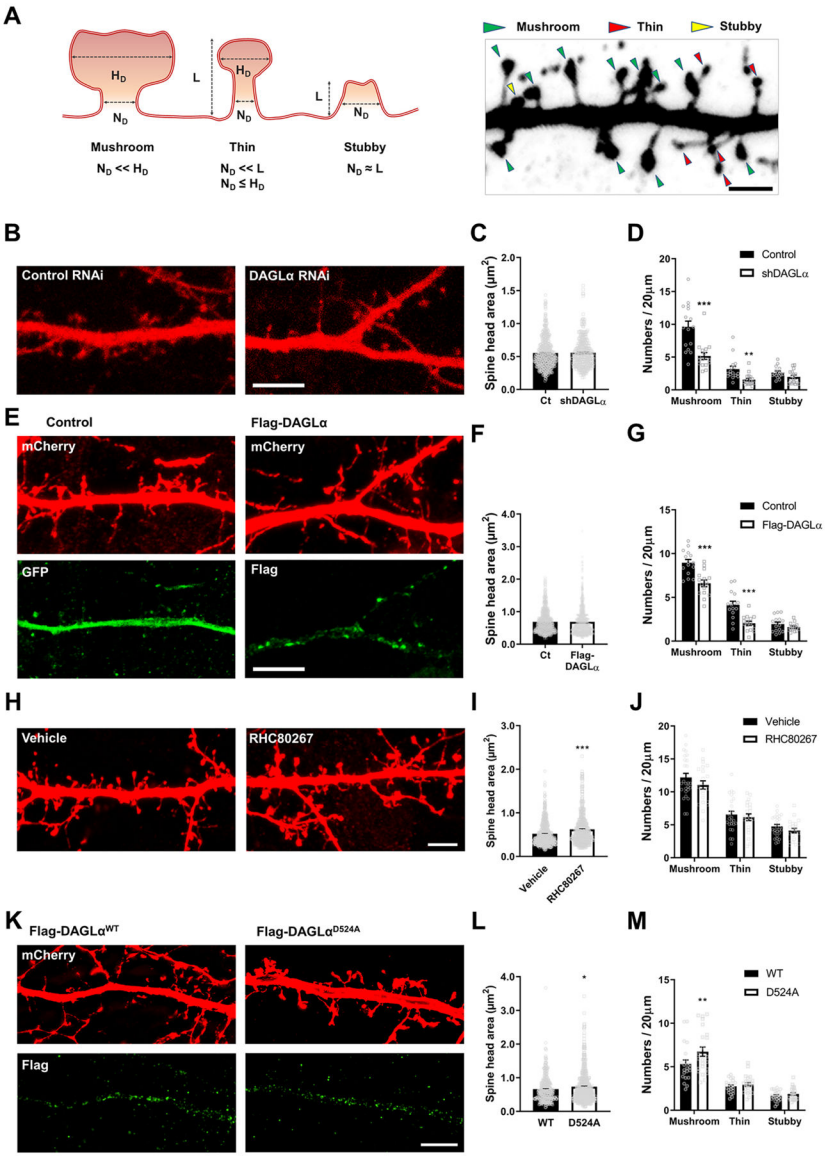


**Figure 1. DAGLα regulates spine development.**

(**A**) Dendritic spines were categorized into mushroom, thin, and stubby spines. A diagram of dendritic spines (left) and a representative image of spine analysis (right) were shown. L, length; $N_D$, the diameter of the spine neck; $H_D$, the diameter of the spine head. (**B**) Confocal images of neurons transfecting mCherry expressing scramble (control RNAi) or DAGLα RNAi (shDAGLα) construct. Scale bar, 5 μm. (**C**) Bar graph showing the spine head size of mushroom types in control or shDAGLα. n = 16 neurons per group. (**D**) Bar graph showing spine density for each shape. **p = 0.002; ***p < 0.001; Two-tailed unpaired t-test. (**E**) Confocal images of neurons expressing mCherry + GFP (Control) or mCherry + Flag-DAGLα (Flag-DAGLα) construct (top panel). Flag-DAGLα expression was confirmed by α-Flag antibody conjugated DyLight488 (bottom panel). Scale bar, 5 μm. (**F**) Bar graph showing the spine head size of mushroom types in control or Flag-DAGLα. n = 15 neurons per group. (**G**) Bar graph showing spine density for each shape. ***p < 0.001; Two-tailed

unpaired t-test. (**H**) Confocal images of mCherry expressing neurons after treatment of RHC80267 (10 μM), an inhibitor of 2-AG formation, for 1 hour. Scale bar, 5 μm. (**I**) Bar graph showing spine head size of mushroom types in vehicle or RHC80267. n = 26 neurons from vehicle and n = 21 neurons from RHC80267. ***p < 0.001; Two-tailed unpaired t-test. (**J**) Bar graph showing spine density for each shape. (**K**) SIM images of neurons expressing mCherry + Flag-DAGLα$^{WT}$ or mCherry + Flag-DAGLα$^{D524A}$ construct for 3 days. Scale bar, 5 μm. (**L**) Bar graph showing spine head size of mushroom types in WT or D524A. n = 22 neurons from WT and n = 23 neurons from D524A. *p = 0.0103; Two-tailed unpaired t-test was performed. (**M**) Bar graph showing spine density for each shape. **p = 0.006; Two-tailed unpaired t-test. All data are represented as mean ± SEM. Ct: control. See also Figure S1 and Table S2.

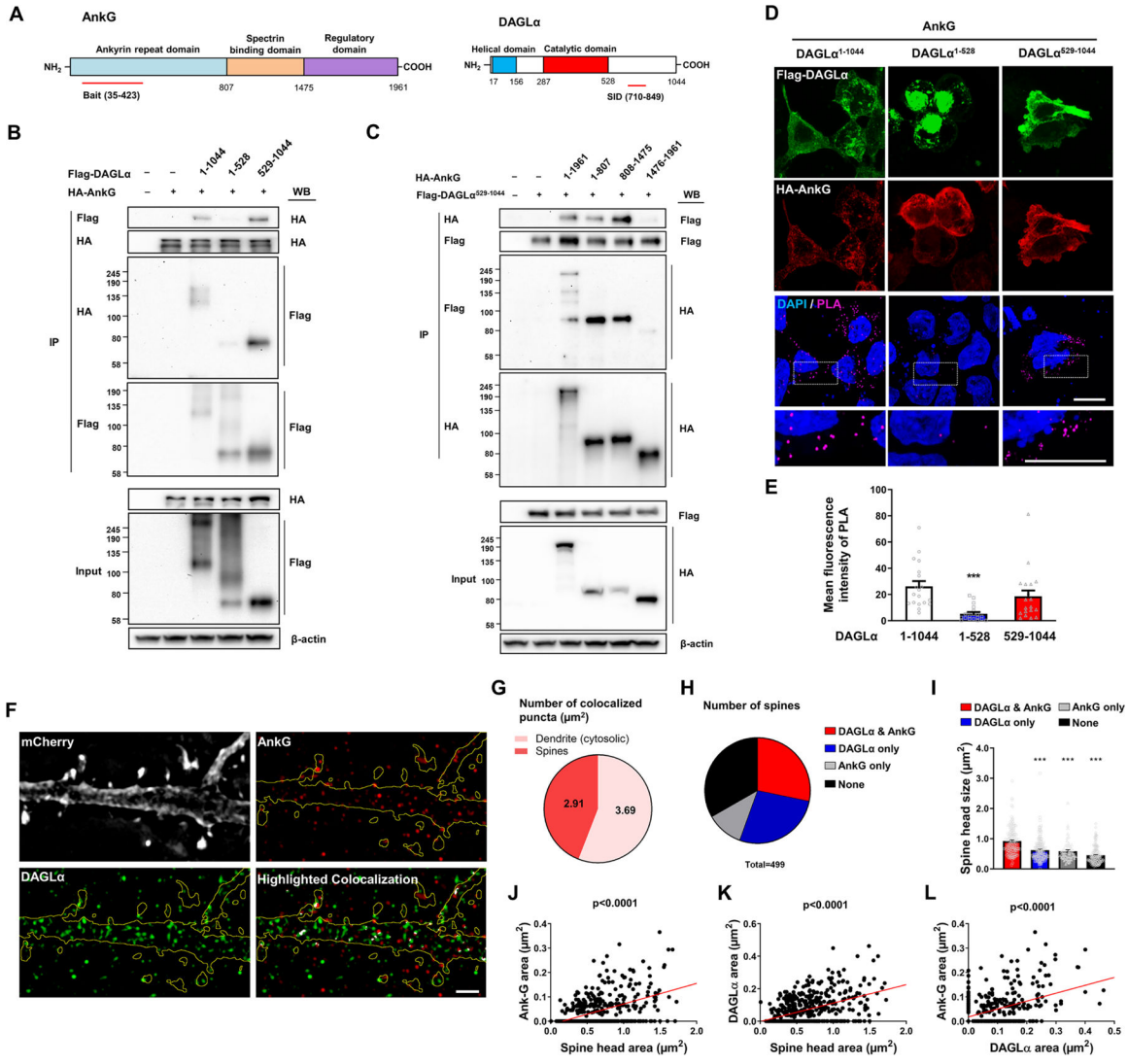


**Figure 2. Super-resolution imaging of spatial organization of ankyrin-G and DAGLα relationship within spine architecture.**

**(A)** Schematic representation of the interaction domain of DAGLα with ankyrin-G from a yeast 2-hybrid screen. A part of ankyrin 24 repeats domain was used as a bait fragment. SID, Selected Interaction Domain. (**B-C**) Binding of DAGLα or ankyrin-G and its subfragments to ankyrin-G or DAGLα in HEK293T cells. The cell lysate was analyzed by immunoblotting with HA or Flag antibody. IP, immunoprecipitation. (**D**) Confocal images for detection of interaction between HA-AnkG and Flag-DAGLα$^{1-1044}$ or Flag-DAGLα$^{1-528}$ or Flag-DAGLα$^{529-1044}$ with *in situ* proximity ligation assay (PLA) from HEK293T cells. Scale bar, 20 μm. (**E**) Bar graph of PLA signal with the truncated mutants of Flag-DAGLα and HA-AnkG expressing cells. n = 19 cells per each group. ***p = 0.0004; One-way ANOVA was followed by Bonferroni post-tests. (**F**) SIM image of mCherry-expressing neurons immunostained for anti-ankyrin-G (red) and anti-DAGLα (green). Scale bar, 2 μm. The co-stained proteins were analyzed with the colocalization highlighter feature in ImageJ, shown in white. (**G**) Pie chart showing the highlighted

colocalized puncta ratio of spines versus dendrites per area of the spine. (**H**) Expression patterns of ankyrin-G and DAGLα in spine shown by pie chart. (**I**) Spine head size from the chart (H) analyzed with a bar graph. ***$p < 0.001$; One-way ANOVA was followed by a Bonferroni test. (**J**-**L**) Correlation plot of the number of anti-ankyrin-G or anti-DAGLα nanodomains versus spine head area. 18 neurons were analyzed. All data are represented as mean ± SEM. See also Figure S2 and Table S1.

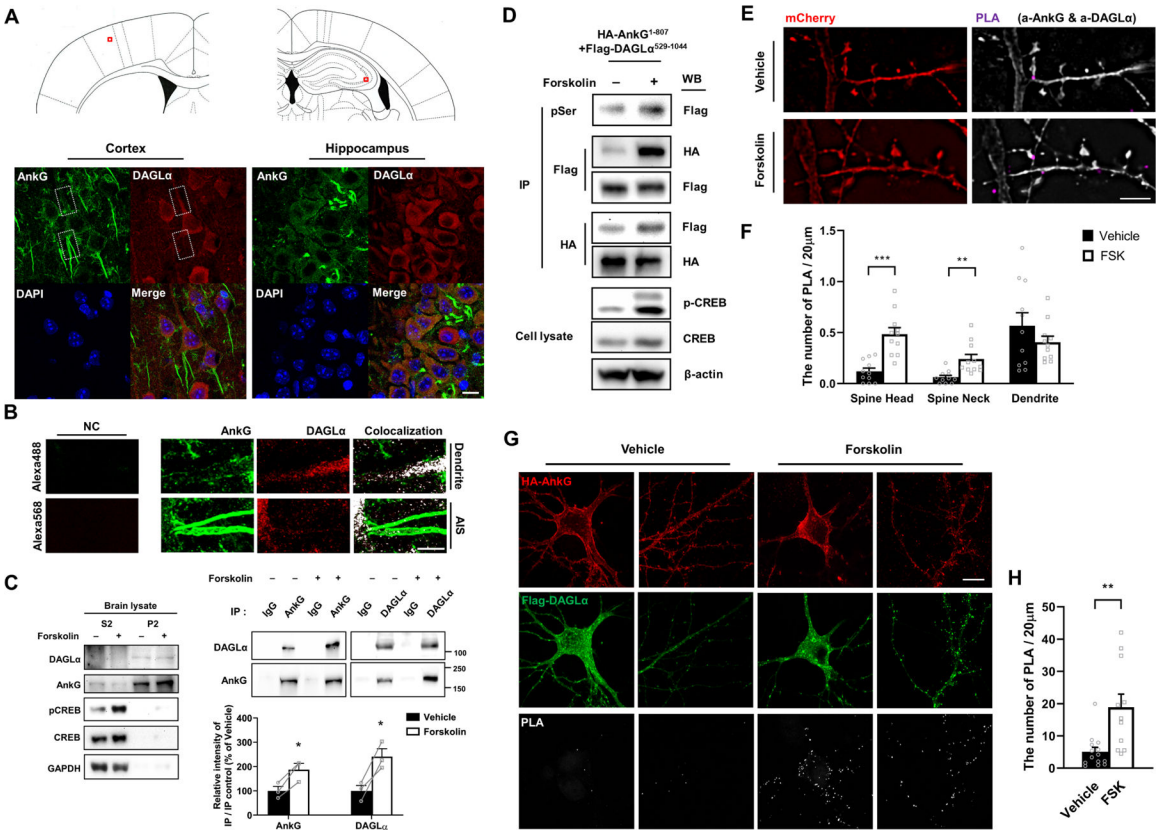


**Figure 3. Forskolin-mediated phosphorylation of DAGLα enhances its interaction with ankyrin-G.**

(**A**) Staining in the primary somatosensory cortex and hippocampus of the 12-week old mouse brain (top panel); magnified layer II-III and CA3 were zoomed into cell level (bottom panel). Scale bar, 10 μm. (**B**) Colocalization of ankyrin-G and DAGLα in the dendrite and AIS from the dotted box of (A) were highlighted by ImageJ. Scale bar, 5μm. NC: negative control. (**C**) Western blots of co-immunoprecipitation experiments of ankyrin-G with DAGLα. Protein samples were obtained from the 12-week old mouse cortex. Mice were injected vehicle or forskolin (1mg/kg) by i.p. and sacrificed 30 min after injection. IgG, control IgG; IP, immunoprecipitation; S2, cytosolic proteins; P2, membrane-associated proteins. n = 3 mice per each group. *$p < 0.05$; Two-tailed unpaired t-test. All data are represented as mean ± SEM. (**D**) Representative western blot of the HA-AnkG$^{1-807}$ with coexpressing Flag-DAGLα$^{529-1044}$ construct. The transfected HEK293T cells were treated with 30 μM of forskolin for an additional 30 min before harvesting. Phosphorylated CREB was detected for forskolin positive signaling. (**E**) SIM image of the mCherry-expressing neuron to detect the interaction between ankyrin-G and DAGLα by PLA (magenta). Scale bar, 5 μm. (**F**) The number of PLA puncta in dendrites after treatment of vehicle or forskolin shown by bar graph. n = 11 neurons per each group. **$p < 0.01$; ***$p < 0.001$; Two-tailed unpaired t-test. (**G**) Confocal images of primary cortical neurons for detection of interaction between HA-AnkG and Flag-DAGLα with PLA after treatment with vehicle or forskolin (30 μM) for 30 min before fixation. Scale bar, 10 μm. (**H**) The number of puncta per 20 μm in dendrites from (G) shown by bar graph. n = 14 neurons from vehicle and n = 11 neurons

from forskolin. **p < 0.01; Two-tailed unpaired t-test. All data are represented as mean ± SEM. FSK: forskolin. See also Figure S3 and Table S1.

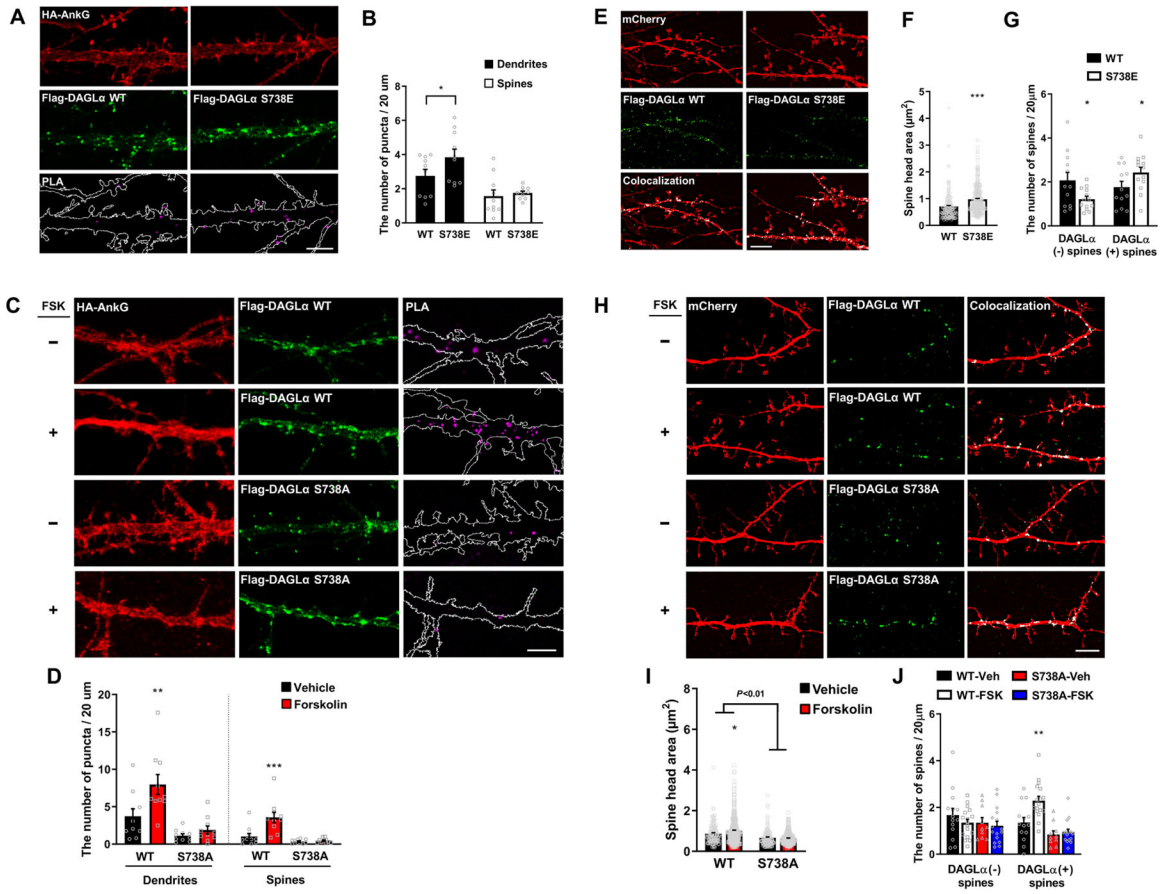


**Figure 4. Forskolin-mediated phosphorylation of DAGLα via serine 738 enhances the interaction with ankyrin-G and regulates spine morphology.**

(**A-D**) SIM images of primary cortical neurons for detection of interaction between HA-AnkG and Flag-DAGLα WT or S738E (A) or S738A (C) with PLA. Dendrite outlined in white following HA-AnkG expression. Scale bar, 5 μm. The density of PLA puncta in dendritic shaft or spines (B,D). n = 10 neurons per each group. *p = 0.045; Two-tailed unpaired t-test was performed for WT versus S738E (B). **p = 0.005; ***p < 0.001; One-way ANOVA was followed by Bonferroni post-tests for WT versus S738A (D). (**E-J**) SIM images of cortical neurons (E, H). Scale bar, 5 μm. Bar graphs of spine head size (F, I) and density (G, J). WT, n = 12; S738E, n = 13; WT-Veh, n = 14; WT-FSK, n = 7; S738A-Veh, n = 10; S738A-FSK, n = 16. Veh: vehicle. *p < 0.05; ***p < 0.0001; Two-tailed unpaired t-test was performed for WT versus S738E. *p = 0.037; **p = 0.0042; Two-way ANOVA was followed by Bonferroni post-tests for WT versus S738A. All data represent mean ± SEM. See also Figure S4, and Tables S1 and S2.

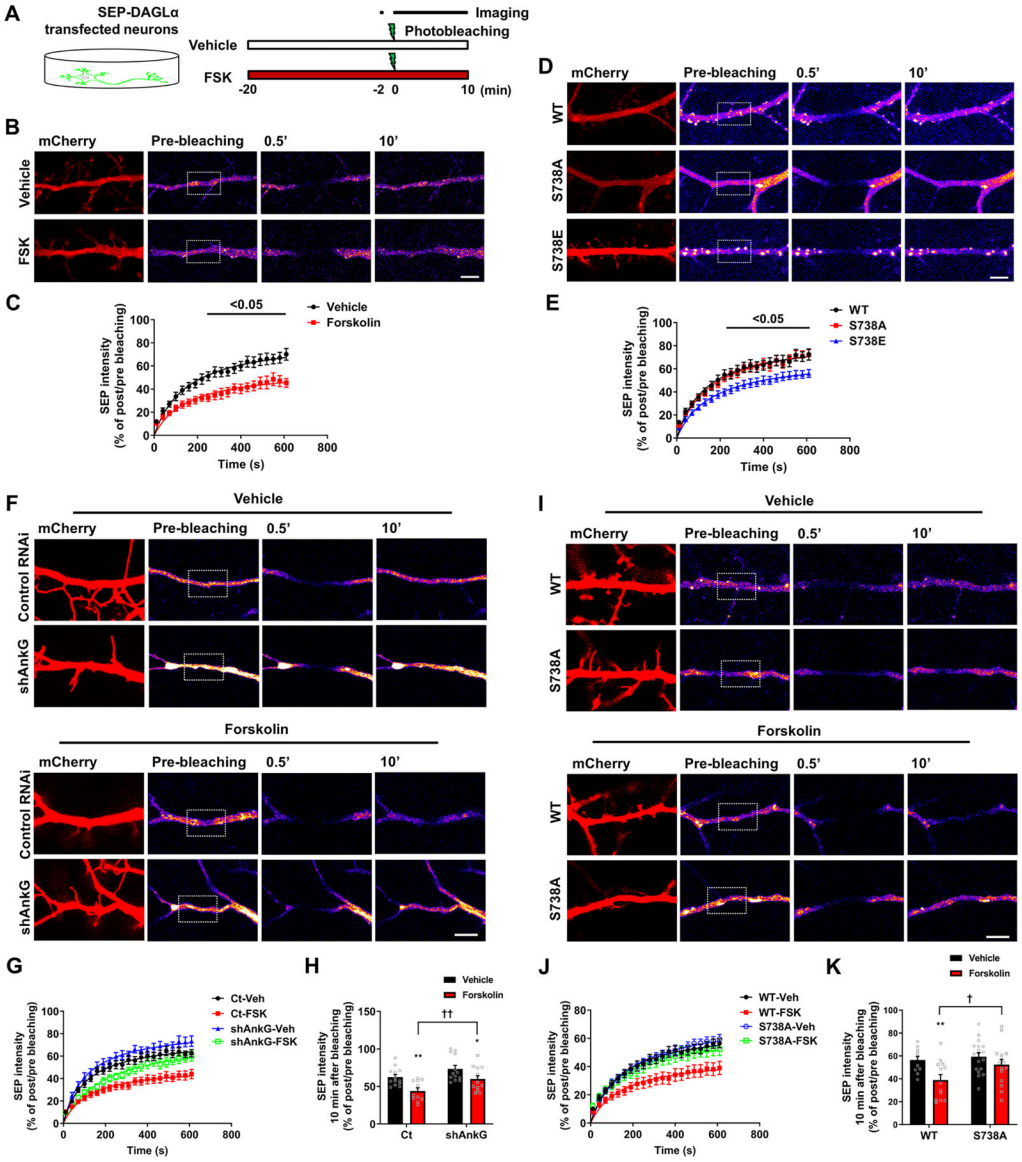


**Figure 5. Ankyrin-G regulates pS738-mediated surface diffusion of DAGLα.**

(**A**) Experimental design. FSK: forskolin. (**B**) Time-lapse images following photobleaching of the dendritic shaft with SEP-DAGLα. The dotted white box indicates the dendritic site that has undergone photobleaching. Scale bar, 5 μm. (**C**) Distinct fluorescence recovery on dendrites with SEP-DAGLα, with and without FSK. n = 12 neurons per each group. Two-way ANOVA was followed by Bonferroni post-tests. (**D**) Time-lapse images following photobleaching of dendritic shaft with SEP-DAGLα WT or S738A or S738E. The dotted white box indicates the dendritic site that has undergone photobleaching. Scale bar, 5 μm. (**E**) Distinct fluorescence recovery on dendrites with SEP-DAGLα WT or S738A or S738E. n = 16 neurons per each group. Two-way ANOVA was followed by Bonferroni post-tests. (**F**) Time-lapse images of SEP-DAGLα following photobleaching of dendritic shaft with control RNAi or ankyrin-G RNAi (shAnkG) in vehicle (top panel) and FSK (bottom panel). The dotted white box indicates the dendritic site that has undergone photobleaching. Scale

bar, 5 μm. (**G**) Distinct fluorescence recovery of SEP-DAGLα on dendrites with control RNAi or shAnkyrin-G, and FSK or vehicle. (**H**) Fluorescence recovery of SEP-DAGLα on dendrites with control RNAi or shAnkG, and FSK or vehicle. Ct-Veh, n = 13; Ct-FSK, n = 11; shAnkG-Veh, n =13; shAnkG-FSK, n = 13. Veh: vehicle.. *p = 0.033; **p = 0.001; $^{\dagger\dagger}$p = 0.009; Two-way ANOVA was followed by Bonferroni post-tests. Ct: control RNAi. (**I**) Time-lapse images of SEP-DAGLα WT or S738A following photobleaching dendritic shaft with vehicle or forskolin treatment. The dotted white box indicates the dendritic site that has undergone photobleaching. Scale bar, 5 μm. (**J**) Distinct fluorescence recovery of SEP-DAGLα WT or S738A on dendrites with vehicle or forskolin treatment. (**K**) Fluorescence recovery of SEP-DAGLα WT or S738A on dendrites with vehicle or forskolin treatment. WT-Veh, n = 11; WT-FSK, n = 13; S738A-Veh, n = 18; S738A-FSK, n = 15. **p = 0.008; $^{\dagger}$p = 0.044; Two-way ANOVA was followed by Bonferroni post-tests. All data are represented as mean ± SEM. See also Figure S5 and Table S1.

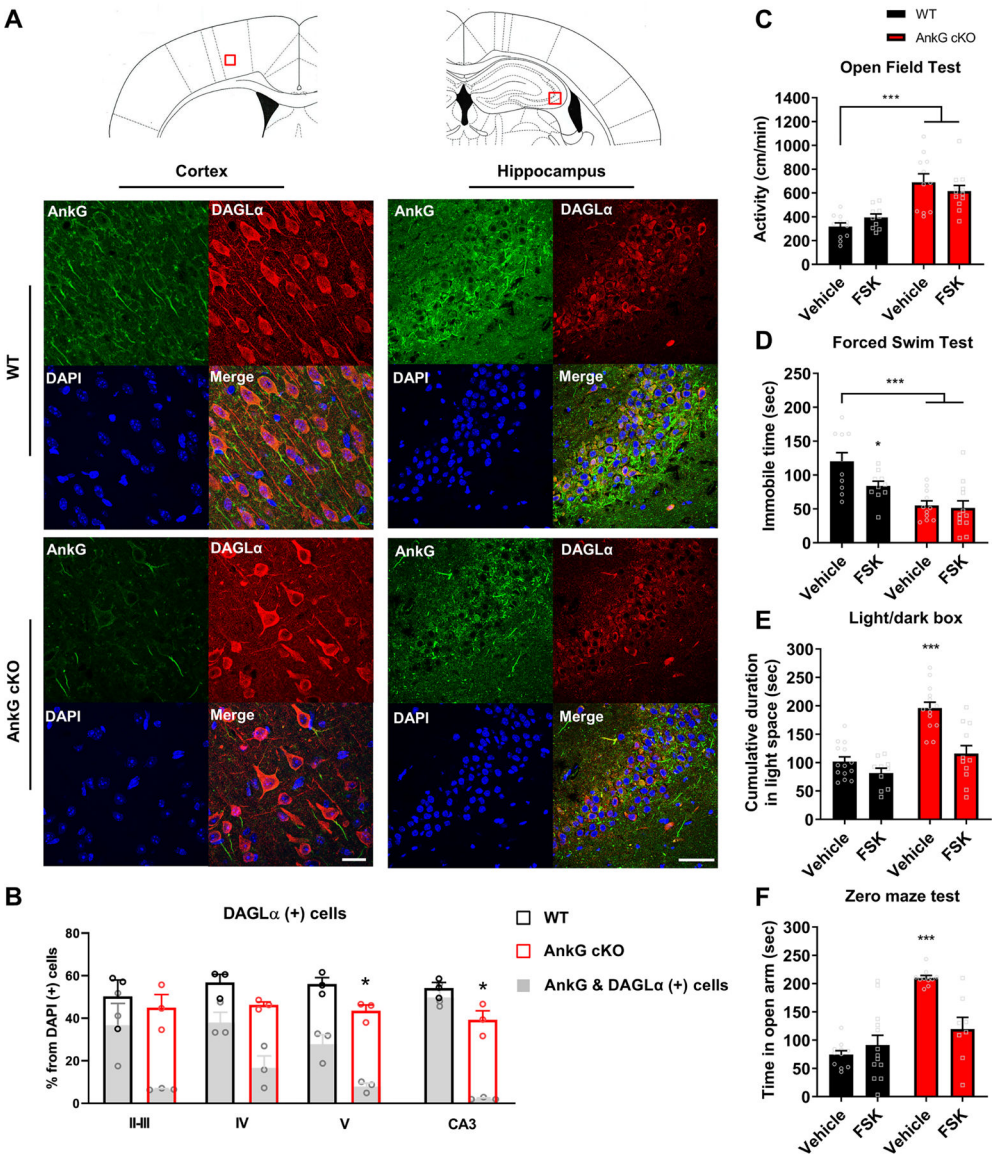


**Figure 6. Absence of ankyrin-G alters behavioral responses induced by forskolin.**

(**A**) Representative images of double-immunohistochemical staining with ankyrin-G (detected in green) and DAGLα (detected in red) in the primary somatosensory cortex (Bregma 0.50 mm) and the hippocampus (Bregma - 1.70mm) of the 12-week old mouse brain. Layer V-specific expression patterns of ankyrin-G and DAGLα are shown in the left panel (Scale bar, 20μm) and CA3 of the hippocampus is shown in the right panel (Scale bar, 200μm) as representative images. (**B**) The fraction of DAGLα-positive or ankyrin-G & DAGLα-positive cells and quantification (n = 3 per each group) in each layer of the cortex (left) and CA3 of the hippocampus (right). The graph is shown with mean values. *p < 0.05; followed by two-tailed unpaired Student's t-test. (**C**) Open-field test for 30 min. WT with vehicle, n = 11; WT with forskolin (FSK), n = 10; AnkG cKO with vehicle, n = 11; AnkG cKO with FSK, n = 12. ***p < 0.001; one-way ANOVA was followed by Bonferroni post-tests. (**D**) Immobility was assessed in adult mice in the forced swim test for 4 min. WT

with vehicle, n = 11; WT with FSK, n = 10; AnkG cKO with vehicle, n = 11; AnkG cKO with FSK, n = 12. *p < 0.05; ***p < 0.001; one-way ANOVA was followed by Bonferroni post-tests. (**E**) Light/dark box test for 5 min. Time in light space is shown by graph. WT with vehicle, n = 14; WT with FSK, n = 10; AnkG cKO with vehicle, n = 14; AnkG cKO with FSK, n = 12. ***p < 0.001; one-way ANOVA was followed by Bonferroni post-tests. (**F**) Zero maze test for 5 min. Time in the open arm is shown by graph. WT with vehicle, n = 11; WT with FSK, n = 13; AnkG cKO with vehicle, n = 11; AnkG cKO with FSK, n = 18. ***p < 0.001; one-way ANOVA was followed by Bonferroni post-tests. All data are represented as mean ± SEM. All mice were injected with vehicle or forskolin (0.2 mg/kg) by i.p. and each behavioral test was conducted 30 min after injection. See also Figure S6 and S7.

**Table 1.**
**Detection of DAGLα phosphorylation sites.**

Flag-DAGLα$^{529-1044}$ was immunoprecipitated from HEK293T cell lysates after treatment with forskolin (30 μM for 30 min) in the absence or presence of Rp-8-Br-cAMPS (PKA inhibitor, 500 μM for 1 hr) preincubation. The table lists the ion scores of phosphorylated residues as analyzed by Mascot. “ND” indicates that the peptide was detected, but phosphorylation was not present.

| Residue | Vehicle | Forskolin | Rp-8-Br-cAMP + Forskolin |
|---|---|---|---|
| Ser728 | 9 | 8 | 10 |
| **Ser738** | **1** | **17** | **1** |
| Ser750 | ND | ND | 3 |
| Ser774 | 26 | 6 | 6 |
| **Ser808** | **ND** | **6** | **ND** |
| Ser810 | ND | ND | 14 |
| Thr830 | ND | ND | 5 |
| Ser837 | ND | ND | 5 |
| **Ser954** | **ND** | **18** | **ND** |
| **Ser956** | **ND** | **5** | **ND** |
| ThrlO23 | ND | 58 | 56 |

*Biol Psychiatry*. Author manuscript; available in PMC 2022 August 15.

KEY RESOURCES TABLE

| Resource Type | Specific Reagent or Resource | Source or Reference | Identifiers | Additional Information |
|---|---|---|---|---|
| Add additional rows as needed for each resource type | Include species and sex when applicable. | Include name of manufacturer, company, repository, individual, or research lab. Include PMID or DOI for references; use “this paper” if new. | Include catalog numbers, stock numbers, database IDs or accession numbers, and/or RRIDs. RRIDs are highly encouraged; search for RRIDs at https://scicrunch.org/resources. | Include any additional information or notes if necessary. |
| Antibody | Mouse monoclonal anti-AnkG | NeuroMab Facility | Cat#75–146; RRID: AB_10673030 | ICC, PLA, IHC (1:200) |
| Antibody | Rabbit polyclonal anti-AnkG (H-215) | Santa Cruz Biotechnology | Cat# sc-28561; RRID: AB_633909 | WB (1:200) |
| Antibody | Goat polyclonal anti-AnkG (P-20) | Santa Cruz Biotechnology | Cat#sc-31778; RRID: AB _2289736 | WB (1:200) |
| Antibody | Rabbit polyclonal anti-DAGLα | Bioss | Cat#bs-11833R | ICC, PLA, IHC (1:200) |
| Antibody | Goat polyclonal anti-DAGLα | Abcam | Cat#ab81984; RRID: AB_1658310 | WB (1:1,000) |
| Antibody | Goat polyclonal anti-PSD95 | Abcam | Cat#ab12093; RRID: AB _298846 | ICC (1:500) |
| Antibody | Chicken polyclonal anti-MAP2 | Abcam | Cat#ab15452; RRID: AB _805385 | ICC (1:1,000), IHC (1:500) |
| Antibody | Mouse monoclonal anti-Bassoon (clone SAP7F407) | Abcam | Cat#ab82958; RRID: AB _1860018 | ICC (1:1,000) |
| Antibody | Mouse monoclonal anti-Na, K-ATPase alpha 1 | Novus | Cat#NB300–146SS; RRID: AB_1290564 | WB (1:1,000) |
| Antibody | Mouse monoclonal anti-Flag (clone M2) | Sigma-Aldrich | Cat#F1804; RRID: AB _262044 | IP (3μg), WB (1:1,000) |
| Antibody | Mouse monoclonal anti-HA (clone HA-7) | Sigma-Aldrich | Cat#H3663; RRID: AB _262051 | IP (3μg) |
| Antibody | Rabbit polyclonal anti-HA | Enzo Life Sciences | Cat#ADI-MSA-106; RRID: AB _10615792 | WB (1:1,000) |
| Antibody | Mouse monoclonal anti-β-actin (clone AC-74) | Sigma-Aldrich | Cat#A2228; RRID: AB _476697 | WB (1:10,000) |
| Antibody | Chicken polyclonal anti-mCherry | Abcam | Cat#ab205402; RRID: AB_2722769 | ICC (1:1,000) |
| Antibody | Goat polyclonal anti-mCherry | SICGEN | Cat#AB0040; RRID: AB_2333092 | WB (1:1,000) |
| Antibody | Rabbit monoclonal anti-p-CREB (Ser133) | Cell signaling Technology | Cat#9198; RRID: AB_2561044 | ICC (1:800), WB (1:1,000) |
| Antibody | Mouse monoclonal anti-CREB (86B10) | Cell signaling Technology | Cat#9104; RRID: AB _490881 | WB (1:1,000) |
| Antibody | Rabbit polyclonal anti-phosphoserine | Abcam | Cat#ab9332; RRID: AB _307184 | IP (3μg) |
| Antibody | Mouse monoclonal anti-Flag-488 (clone M2) | Abcam | Cat#ab117505; RRID: AB _10972518 | ICC, PLA (1:500) |
| Antibody | Rabbit polyclonal anti-HA-568 | Synaptic System | Cat#245 003C3; RRID: AB _2619954 | PLA (1:500) |
| Antibody | Chicken polyclonal anti-GFP | Abcam | Cat#ab13970; RRID: AB _300798 | ICC (1:10,000) |
| Antibody | Goat anti-mouse 488 | Thermo Fisher Scientific | Cat#A-11029; RRID: AB _2534088 | ICC (1:1,000) |
| Antibody | Donkey anti-rabbit 488 | Thermo Fisher Scientific | Cat#A-21206; RRID: AB _2535792 | ICC (1:1,000) |

| Resource Type | Specific Reagent or Resource | Source or Reference | Identifiers | Additional Information |
|---|---|---|---|---|
| Antibody | Donkey anti-rabbit 568 | Thermo Fisher Scientific | Cat#A-10042; RRID: AB _2534017 | ICC (1:1,000) |
| Antibody | Goat anti-chicken 568 | Thermo Fisher Scientific | Cat#A-11041; RRID: AB _2534098 | ICC (1:1,000) |
| Antibody | Goat anti-mouse 568 | Thermo Fisher Scientific | Cat#A-11031; RRID: AB _144696 | ICC (1:1,000) |
| Antibody | Donkey anti-goat 647 | Thermo Fisher Scientific | Cat#A-21447; RRID: AB _2535864 | ICC (1:1,000) |
| Antibody | Goat anti-chicken 647 | Thermo Fisher Scientific | Cat#A-21449; RRID: AB _2535866 | ICC (1:1,000) |
| Antibody | Donkey anti-mouse 647 | Thermo Fisher Scientific | Cat#A-31571; RRID: AB _162542 | ICC (1:1,000) |
| Bacterial or Viral Strain | E. coli HST08 | TaKaRa | #636766 | DNA amplification |
| Cell Line | HEK293T/17 cells | ATCC | #CRL-11268 | |
| Commercial Assay Or Kit | Duolink® In Situ PLA® Probe Anti-Mouse MINUS | Sigma | #DUO92004 | PLA |
| Commercial Assay Or Kit | Duolink® In Situ PLA® Probe Anti-Rabbit PLUS | Sigma | #DUO92002 | PLA |
| Commercial Assay Or Kit | Duolink® In Situ Detection Reagents FarRed | Sigma | #DUO92013 | PLA |
| Commercial Assay Or Kit | Phire Animal Tissue Direct PCR Master Kit | Thermo Fisher Scientific | Cat#F140WH | Genotyping |
| Genetic Reagent | In-Fusion® HD Cloning Plus | Clontech | #638911 | Cloning |
| Genetic Reagent | QuickChange Site-Directed Mutagenesis Kit | Agilent Technologies | #200516 | Point mutation |
| Organism/Strain | C57BL/6J (Male) | Jackson Laboratory | #000664 | IP, primary culture |
| Organism/Strain | Mouse: AnkG loxP | The Jackson Laboratory | #029797 | IHC, Behaviors |
| Organism/Strain | Mouse: Camk2α-cre | The Jackson Laboratory | #005359 | IHC, Behaviors |
| Recombinant DNA | pEZ-3XHA-AnkG | GeneCopoeia | Cat# EX-Mm25668-M06 | |
| Recombinant DNA | pEZ-3XFlag-DAGLα | GeneCopoeia | Cat#EX-Mm36327-M12 | |
| Recombinant DNA | psi-mU6 Control RNAi | GeneCopoeia | Cat#CSHCTR001–1-mU6 | |
| Recombinant DNA | psi-mU6 shDAGLα | GeneCopoeia | Cat# MSH043012–2-mU6 | |
| Recombinant DNA | psi-mU6.1 shAnkG | GeneCopoeia | Cat# MSH038708–33-mU6 | |
| Recombinant DNA | pmCherry-C1 | Clontech | Cat#632524 | |
| Recombinant DNA | pEZ-3XHA-AnkG1–807 | Yoon et al., 2020 | N/A | |
| Recombinant DNA | pEZ-3XHA-AnkG808–1475 | Yoon et al., 2020 | N/A | |
| Recombinant DNA | pEZ-3XHA-AnkG1476–1961 | Yoon et al., 2020 | N/A | |
| Recombinant DNA | pEZ-3XFlag-DAGLα1–528 | This paper | N/A | |
| Recombinant DNA | pEZ-3XFlag-DAGLα529–1044 | This paper | N/A | |

| Resource Type | Specific Reagent or Resource | Source or Reference | Identifiers | Additional Information |
|---|---|---|---|---|
| Recombinant DNA | pSEP-DAGLα | This paper | N/A | |
| Recombinant DNA | pEGFP-DAGLα | This paper | N/A | |
| Recombinant DNA | pEZ-3XFlag-DAGLα529–1044 S738A | This paper | N/A | |
| Recombinant DNA | pEZ-3XFlag-DAGLα529–1044 S808A | This paper | N/A | |
| Recombinant DNA | pEZ-3XFlag-DAGLα529–1044 S738;808A | This paper | N/A | |
| Recombinant DNA | pEZ-3XFlag-DAGLα529–1044 S738E | This paper | N/A | |
| Recombinant DNA | pEZ-3XFlag-DAGLα529–1044 S808E | This paper | N/A | |
| Recombinant DNA | pEZ-3XFlag-DAGLα529–1044 S738;808E | This paper | N/A | |
| Recombinant DNA | pEZ-3XFlag-DAGLα S524A | This paper | N/A | |
| Recombinant DNA | pEZ-3XFlag-DAGLα S738A | This paper | N/A | |
| Recombinant DNA | pEZ-3XFlag-DAGLα S738E | This paper | N/A | |
| Recombinant DNA | pEZ-3XFlag-DAGLα529–1044 S954A | This paper | N/A | |
| Recombinant DNA | pEZ-3XFlag-DAGLα529–1044 S956A | This paper | N/A | |
| Recombinant DNA | pEZ-3XFlag-DAGLα529–1044 S954;956A | This paper | N/A | |
| Recombinant DNA | pEZ-3XFlag-DAGLα529–1044 S954E | This paper | N/A | |
| Recombinant DNA | pEZ-3XFlag-DAGLα529–1044 S956E | This paper | N/A | |
| Recombinant DNA | pEZ-3XFlag-DAGLα529–1044 S954;956E | This paper | N/A | |
| Recombinant DNA | pSEP-DAGLα S738A | This paper | N/A | |
| Recombinant DNA | pSEP-DAGLα S738E | This paper | N/A | |
| Software; Algorithm | FIJI (ImageJ) | NIH | https://fiji.sc/ | |
| Software; Algorithm | NIS-Elements v4.51.00 | Nikon | http://www.nikon.com/products/microscope-solutions/support/index.htm | |
| Software; Algorithm | Prism 8 | GraphPad | http://www.graphpad.com/scientific-software/prism/ | |
| Software; Algorithm | Image Lab 3.0 | Bio-Rad Laboratories | http://www.bio-rad.com/en-us/product/image-lab-software | |
| Software; Algorithm | EthoVision XT 11.5 | Noldus | http://www.noldus.com | |
| Chemicals | Forskolin | Cell signaling Technology | Cat#3828 | |
| Chemicals | RHC 80267 | Tocris | Cat#1842 | |